Journal of Materials Processing Technology 245 (2017) 15–23

Contents lists available at ScienceDirect

Journal of Materials Processing Technology

journal homepage: www.elsevier.com/locate/jmatprotec

Arc characteristics and metal transfer behavior in narrow gap gas metal arc welding process

Gang Zhang, Yu Shi*, Ming Zhu, Ding Fan

State Key Laboratory of Advanced Processing and Recycling Non-ferrous Metals, Lanzhou University of Technology, Lanzhou 730050, China

ARTICLE INFO

Article history:
Received 8 December 2016
Received in revised form 11 February 2017
Accepted 13 February 2017
Available online 16 February 2017

Keywords:
GMAW
Metal transfer
Minimum arc voltage principle
Arc inherent self-regulation
Arc appearance
Narrow gap

ABSTRACT

During the constant-voltage welding machine employed welding process, a common phenomenon of arc attachment point moving from the bottom of the narrow gap to the sidewalls occurs, and metal transfer behavior appears greatly different. A mechanism that the arc inherent-self regulation combines the minimum arc voltage principle was proposed to elaborate the arc climbing up process along the sidewalls. The arc shape was approximately classified into three patterns by the change of arc conductive path, and the amount of the arc conductive path and its distributive symmetry determine the action of the electromagnetic force on the droplet as well as the metal transfer mode. As the number of the arc conductive paths increases, and the conductive paths distribute symmetrically, the necking process of the droplet detachment occurs more easily, and the metal transfer from globular mode to spray mode becomes more smoothly. Simulation results match the experiments and verify the mechanism proposed. In a constant-current welding power source adopted condition, the arc climbing up phenomenon cannot be observed, and a stable welding process is obtained.

1. Introduction

The steel thick walled plates, widely applied in shipbuilding, high-pressure vessels, etc., could be joined with kinds of welding approaches. For instance, Cao et al. (2011) joined 9.3 mm thick butt joints with the hybrid fiber laser-arc welding. Frank et al. (2010) adopted the fiber laser and gas metal arc welding (GMAW) to weld 16 mm and 20 mm thick plates of carbon steel. Gan et al. (2007) reported the friction stir welding of 12.7 mm thick L80 steel. Kiran et al. (2012) studied the effects of process variables on weld quality of HSLA steel using two-wire tandem submerged arc welding (SAW). For a conventional arc welding of the carbon steel thick plates, high-heat input to the work-piece may worsen the joint microstructure and properties, and the weld production requires longer welding time and filler metals that increase weld distortion. However, narrow gap gas metal arc welding (NG-GMAW) is considered as a high-efficient joining method for thick metal plates because of its lower equipment investment, lower heat input, easier operation, less filler metal, and thus less energy consumption, fewer deformation. Guo et al. (2011) investigated the metal transfer behavior in rotating arc narrow gap horizontal welding by changing wire rotating frequency. Xu et al. (2014) studied the microstructure and mechanical properties of high-strength low-alloy steel joints obtained with oscillating arc narrow gap GMAW. Cai et al. (2016) investigated the influences of different shielding gas composition on arc dynamics and metal transfer process.

Investigations point out that the arc characteristics and droplet transfer behavior in the GMAW process mainly determine the stability of welding process and the energy distribution which significantly affects the microstructure and various properties of joints. Comparisons of the conventional GMAW process indicate that the arc appearance of GMAW in the narrow gap is apparently compressed, and the droplet transfer process changes in a more unstable way. Thus, lots of weld defects (i.e., lack of fusion, porosity and slag inclusion) are more likely to generate without taking extra actions that change the arc shape and metal transfer modes. In order to stabilize the dynamic arc in the narrow gap and obtain a sound weld bead, several methods have been currently developed. Yang et al. (2009) developed a rotating arc system to stabilize the sagged weld pool in the narrow gap horizontal welding process. Wang et al. (2012) proposed a swing arc method to alter the arc attachment point and the staying time of the arc on the sidewalls for realizing high-quality narrow gap GMA welding with low cost. Xu et al. (2015) utilized response surface methodology to estimate and optimize the weld bead geometry in oscillating arc narrow gap all-position GMAW. Zhu et al. (2006) developed flux stripes to

* Corresponding author.
E-mail addresses: berscheid@126.com, shiyu@lut.cn (Y. Shi).

http://dx.doi.org/10.1016/j.jmatprotec.2017.02.006
0924-0136/

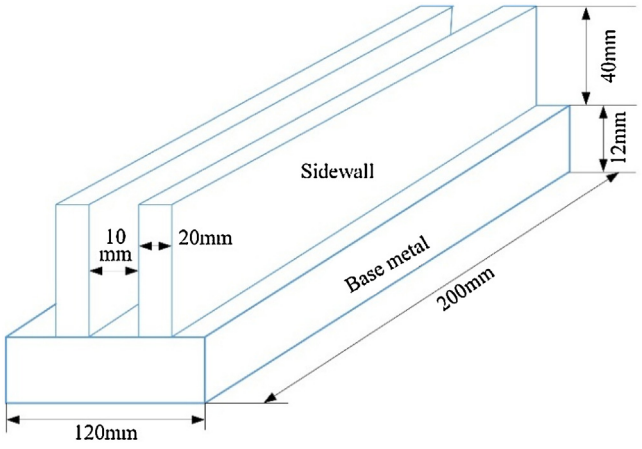

Fig. 1. Dimension of the work-piece.

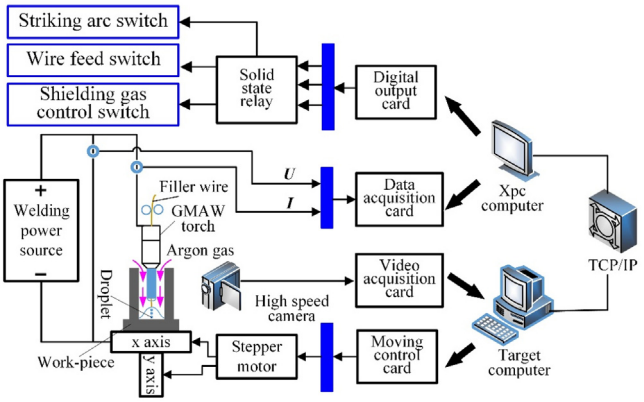

Fig. 2. Rapid prototyping experimental control system.

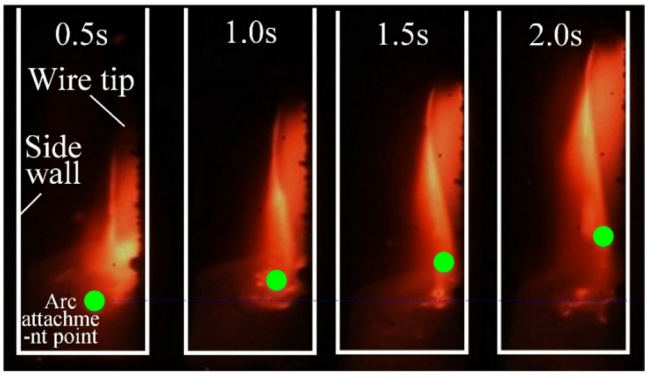

Fig. 3. Typical arc shape images under the CVPS condition.

construct the arc attachment in the ultra-narrow gap welding process and kept the full penetration of the sidewalls. Above-mentioned methods have partly improved the weld bead formation and weld quality. However, the metal transfer behavior and the weld bead forming mechanism in the narrow gap were not deeply studied. With the limit of the author's searching capability, studies on the dynamic arc behavior and metal transfer mechanism in the NG-GMAW process are rarely reported.

This paper focuses on the study of arc characteristics and droplet transfer behavior of the NG-GMAW, and theoretically elaborates on the formation mechanism of the different arc appearance and droplet transfer mode, which are compared with GMAW process. To this end, a high-speed sampling system is developed to capture the arc dynamics and droplet transfer produced by a constant-voltage power source (CVPS) and a constant-current power source (CCPS) respectively. During the CVPS employed welding process, a common phenomenon of the arc attachment point moving to the sidewalls is observed, and its evolvement rules are detailed. The arc model in the narrow gap is also established based on the change of the arc conductive path and is simulated using MATLAB/Simulink platform. This paper is organized by following: an experimental system in Section 2; analysis of the arc characteristics and metal transfer modes and its verification in Section 3 and the results in Section 4.

2. Experimental procedure

Q235 steel was used as the base and sidewall metal. ER50-6 wire with 1.2 mm diameter was used as the filler metal. Pure argon gas (99%) at a flow rate 10 L min^{-1} was utilized to protect the molten pool. The dimension of the work-piece is shown in Fig. 1. In the CVPS case, arc voltage was set 28 V. Welding speed was set 0.325 m min^{-1}, and the wire feed rate was changed from 4.3 m min^{-1} to 7.1 m min^{-1}. The curved wire that will feed in the narrow gap through a wire feeder was previously straightened, and the distance of the wire tip to the two sidewalls was accurately controlled. Welding assistive tools were set to minimize distortion of the weld. The schematic diagram of the experiment system is given in Fig. 2.

This system mainly consists of the welding control, rapid prototyping and video acquisition parts. In the welding control part, a Lincoln Electric® Idealarc® DC-400 CC/CV multi-process welder was applied to generate the heat source for fusing the work-piece and the filler wire, which has two output characteristics, including constant-voltage mode and constant-current mode. A semi-automatic Lincoln LN-7 wire feed machine was employed to control the wire feed speed in the narrow gap welding. The conventional GMAW torch was improved through grinding the width of contact tip and attaching the thin mica sheet on the ground contact tip. To this end, the torch amended can be easily stretched into the narrow gap and be avoided contacting with the sidewalls. Despite the limitation of the narrow gap, the shielding gas nozzle was removed. Hence, to protect the weld pool effectively, another two insulating heat pipes were mounted to the left and right side of the contact tip, and then the pure argon gas was input to the narrow gap. Lu et al. (2012) detailed the rapid prototyping control system as following three parts: the data exchanging section between the target and the host computers; the data-acquisition section; the control section. To acquire the images of arc shape and droplet in the NG-GMAW process, Olympus I-SPEED3 high-speed camera with an Olympus Camera Display Unit was employed. The camera with a speed of up to 15000 frames per second captures the images and stores in its on-board 8GB internal memory storage. Nikon AF-SDX VR 55–200 mm f/4-5.6G IF-ED lens with varying focal lengths was also used to acquire the arc shape and droplet images clearly. The GMA welding torch keeps stationary as the work-piece moves with a pre-setting rate during the entire welding process.

3. Results and discussion

3.1. Arc climbing up phenomenon

Lots of dynamic arc appearance and metal transfer images captured by the high-speed camera were carefully observed and comparatively analyzed with the normal GMAW process. Several typical arc appearance images were shown in Fig. 3. A common phenomenon that the arc attachment point moves to the sidewall is observed in the constant-voltage power source (CVPS) employed GMA welding process. The arc climbs up to the wire tip along the

sidewalls as the filler wire was fed with a constant rate until to melt the contact tip. This process is considered as the climbing up phenomenon of the arc along the sidewalls in the narrow gap welding.

Fig. 3 depicts three apparent points: (1) the arc shape in the narrow gap is drawn out and compressed, which no longer likes a bell shape akin free arc in the GMAW. (2) the arc attachment point moves from the bottom of the narrow gap to the sidewalls, such that it changes the arc conductive path in the narrow gap. (3) the arc attachment point is climbing up along the sidewall until to melt the contact tip when the wire feed rate keeps a constant.

In CVPS employed GMAW process, the arc length can be automatically adjusted by the arc inherent self-regulation as the stable burning arc is disturbed. Unfortunately, this self-regulation of the

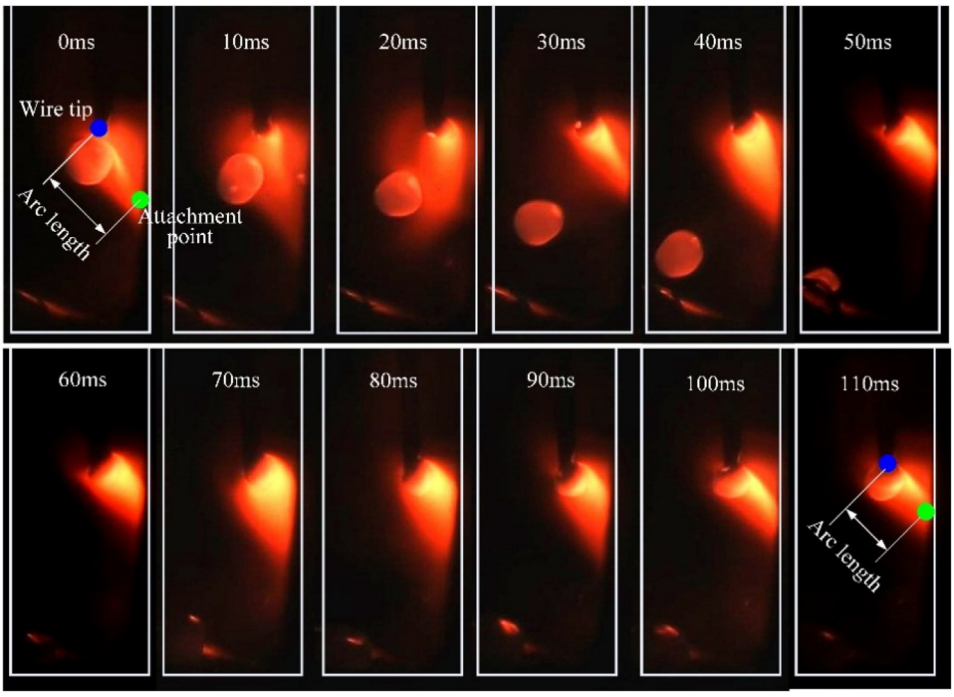

Fig. 4. Droplet images sampled in the first arc shape pattern (V_f = 4.3 m min^{-1}).

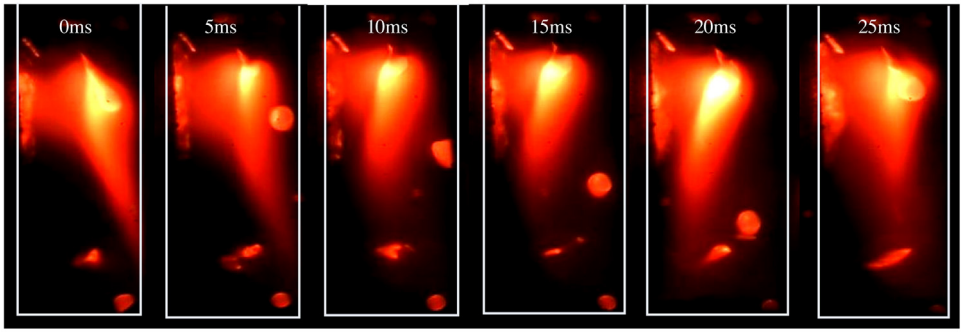

Fig. 5. Droplet images sampled in the second arc shape pattern (V_f = 5.0 m min^{-1}).

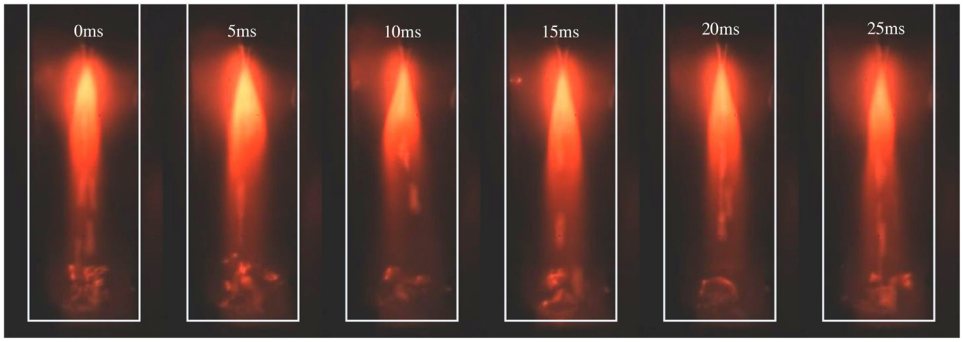

Fig. 6. Droplet images sampled in the third arc shape pattern (V_f = 6.0 m min^{-1}).

arc in the NG-GMAW process failed to achieve the desired result. The reasons are inferred that the arc conductive path may be changed and thus the effect of the inherent self-regulation on the arc length is reduced.

3.2. Arc shape and droplet modes

A set of experiments with different wire feed rate were performed under the CVPS condition. Observations and analysis of the change of the arc shape and the metal transfer process indicate that the moving arc attachment point determines the arc appearance and metal transfer modes, which in turn changes the arc conductive path in the narrow gap. Hence, based on those changes, the arc shape was classified into three patterns.

3.2.1. First pattern

A low wire feed rate was adopted in the experiments, and the droplet detachment images were captured by the high-speed camera with a sampling frequency of 1000 Hz. Some typical images were shown in Fig. 4.

It is apparently observed that the arc only burns between the wire tip and the right sidewall in Fig. 4. The arc length decreases as the arc attachment point climbs up along the sidewall, which can be shown in frames (t = 0 ms and t = 110 ms). Despite using a low wire feed rate and a great arc voltage, the low welding current generates a small electromagnetic force, acting on the droplet. The droplet surface tension depending on the wire chemical compositions prevents the droplet detachment without using the blend shielding gas (active gas and argon gas). Hence, the droplet detachment largely depends on its gravity, and thus the melted wire tip forms a great droplet. The liquid metal transfers from the wire tip to the weld pool by globular mode with 10 Hz frequency which is obtained by manual account. The droplet also detaches off the axis of the arc (shown in frames t = 10 ms ~ 40 ms). The reasons that generate the globular mode in the narrow gap condition are detailed in later section.

3.2.2. Second pattern

The varying arc shape in the narrow gap with the increase of the wire feed rate (from 4.3 m min^{-1} to 5.0 m min^{-1}) was shown in Fig. 5.

Fig. 5 shows that both bottom and sidewall of the narrow gap generate the cathode spot which produces the burning arc between the wire tip to bottom and the sidewall. The arc is originally generated between the wire tip and the right-sidewall. As the welding process continues, the right-side arc gradually climbs up and expands to the left-sidewall, which can be seen in the images (from t = 5 ms to 20 ms). Compared with Fig. 4, the arc becomes unstable due to the random movement of the arc attachment point. Such that, the droplet detachment changes discontinuity and instability. The droplet is transferred by globular mode with 30 Hz frequency, and its detached direction seriously deviates from the axis of the arc. However, the droplet diameter becomes smaller than the first pattern. This is an obvious difference between those two patterns.

3.2.3. Third pattern

Given that the two sidewalls restrain the expansion of the arc, the third arc shape pattern is formed when the arc simultaneously burns between the wire tip to the left and right sidewalls as well as the bottom of the narrow gap. That is to say, three current paths established for stabilizing the arc dynamics. This interesting phenomenon was shown in Fig. 6. Fig. 6 illustrates that the arc is vertically stretched, and the droplet detachment presents the spray transfer mode. The droplet diameter becomes the smallest and the transition frequency increases as the increase of the welding current. Although the transfer process is stable, the axis section of the arc is too narrow to completely cover the bottom of the narrow gap such that the lack of fusion of the sidewalls may easily occur.

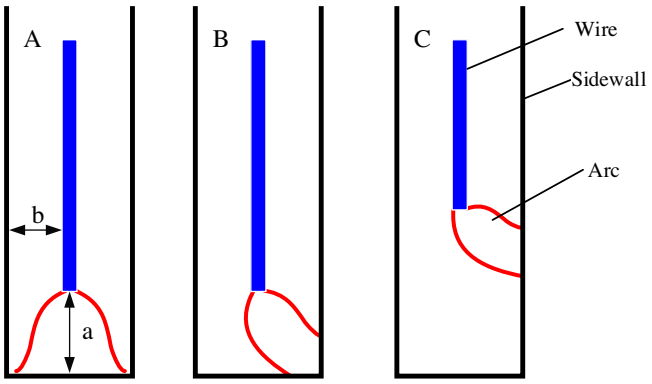

Fig. 7. Simplified arc shape of the NG-GMAW.

3.3. Arc attachment point moving mechanism

To clearly explain the reasons of causing the climbing up phenomenon of the arc in the narrow gap condition, the arc shape showed in Fig. 3 is simplified and its schematic diagram was presented in Fig. 7. The whole movement of the arc attachment point was divided into two processes: the shortening period of the arc length and the climbing up period of the cathode spot.

3.3.1. The first period

Fig. 7A and B show that the wire extension appears to be the same. Only the arc shape changes symmetrical to asymmetrical. Based on the minimum arc voltage principle, it can be easily obtained that the burning arc will automatically choose an appropriate current path to ensure the minimum value of the electric field intensity in the arc column when the welding parameters and other conditions keep constant. Because the electric field intensity of the arc has a percentage ration with the conductive path, the shortest conductive path will be chosen. Fig. 7A also illustrates that the horizontal distance of the wire tip to the left sidewall *b* is shorter than the vertical distance of the wire tip to the bottom of the narrow gap *a*. Hence, the arc appearance changes from status A to B for reducing the conductive path and maintaining a minimum arc voltage. The arc shape is thus considered as being compacted by the sidewalls.

3.3.2. The second period

From the status B to C in Fig. 7, the wire extension has obviously decreased. The arc length and arc shape are also varied. The arc inherent self-regulation greatly affects the stability of the welding process. The illustration is shown in Fig. 8.

In Fig. 8, A_m represents the external characteristic of the welding machine. B_{m1} and B_{m2} denote the static characteristic of long and short arc of the NG-GMAW, respectively. C_m reflects that the wire feed rate equals the wire melting speed.

Given that the arc column is compacted in the first process, the arc length is reduced, and the static characteristic curve is changed from B_{m1} to B_{m2}. Hence, the current melting wire increases from I_{m1} to I_{m2}. The correlation of melting rate with the welding current shows that the melting rate increases, which can be described by $V_{m2} > V_{m1}$. Their correlations can be expressed by the following:

$$V_m = K_i \cdot I - K_u \cdot U \quad (1)$$

Where K_i and K_u refer to the current and the voltage melting coefficients, respectively, whose values are determined by the resistivity, diameter, and wire extension as well as the potential gradient of

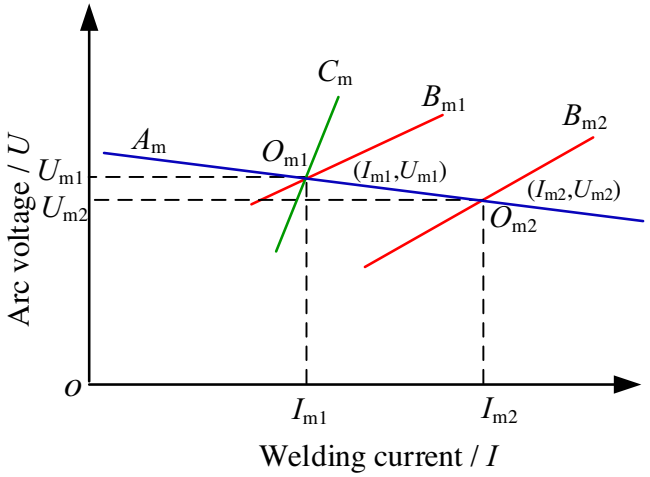

Fig. 8. Diagram of the arc inherent self-regulation under the CVPS condition.

the arc column. The value of them, in this work, is considered as a constant.

When the balance working point of the arc changes from the O_{m1} to O_{m2}, despite the O_{m2} satisfying the characteristic matching requirement between the weld power source and the arc, it cannot meet the balance of the wire feed and the melting speeds. The increased welding current melts more wire, and the arc length increases. However, the horizontal distance b mentioned in Fig. 7 cannot be changed due to the fixed width of the narrow gap, the arc length can only stay the same. Consequently, the new balance point of the arc can only be achieved by regulating the melting rate of the wire. As the wire extension is reduced, the burning arc moves to the conductive nozzle along the sidewalls and ceases the welding process when the conductive nozzle is completely melted. Hence, in the second process, the arc inherent self-regulation has no effect on the adjustment of the varying arc length for stabilizing the arc process. This action leads to the occurrence of the phenomenon of the arc attachment point moving to the sidewalls.

Pre-analysis concludes that the minimum arc voltage principle-based regulation and the arc inherent self-regulation jointly generate the climbing up phenomenon of the burning arc in the CVPS employed narrow gap condition.

3.4. Analysis of metal transfer behavior

3.4.1. Characteristics in the first pattern

The conventional GMAW process analysis concluded that the static force balance theory (detailed by Amson, 1965; Haidar, 1998; Fan and Kovacevic, 2004) can be used to explain why the metal transfer mode changes in the narrow gap GMAW process. To illustrate this transfer mechanism clearly, the arc shape and droplet are approximated in Fig. 9.

As shown in Fig. 9, the forces acting on the droplet include gravity F_g, surface tension F_σ, anode spot pressure F_v, plasma jet force F_a and electromagnetic force F_e. The effect of electromagnetic force on the droplet transfer appears complex due to the varying arc attachment point. When a smaller root area of the arc is formed on the bottom of the droplet, the direction of the electromagnetic force acting on the droplet points upward, which prevents the droplet detachment from the wire tip. Based on the static force balance theory, it can be known that the preventing force F_p combined with F_e, F_σ and F_v, equals to the accelerating force F_{ac} combined with F_g and F_a, which can be expressed by the following Eq. (2):

$$F_g + F_a = F_\sigma + F_v + F_{ey} \quad (2)$$

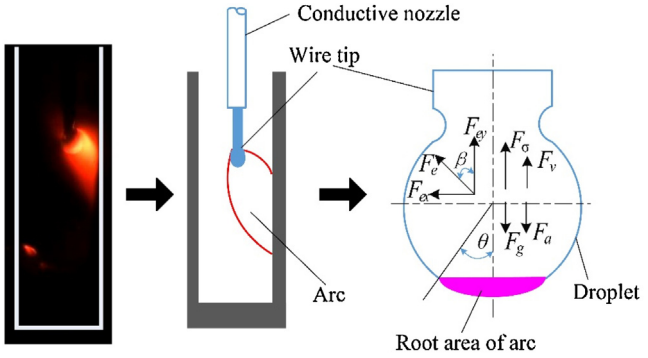

Fig. 9. Simplified arc shape and forces acted on the droplet in the first pattern.

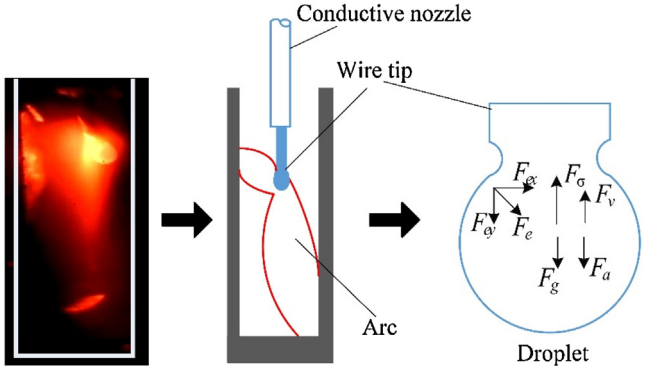

Fig. 10. Simplified arc shape and forces acted on the droplet in the second pattern.

In GMAW process, the electromagnetic force gradually becomes an acceleration force to promote the droplet detachment as the increase of the root area of the arc due to the force direction change ($F_p < F_{ac}$). However, as shown in Fig. 4, the root area of the arc decreases as the arc attachment point climbs up to the wire tip along the sidewall, which changes the direction of the electromagnetic force acted on the droplet, i.e., increasing the angle β (shown in Fig. 9) and decreasing the projection F_{ey} on the y axis (shown in Fig. 9). Hence, the droplet detachment finally depends on its gravity as its size gradually increases, and the droplet transfer mode presents a globular transfer. In addition, the projection F_{ex} on the x axis makes the droplet deviate the vertical direction showed in Fig. 4.

3.4.2. Characteristics in the second pattern

The droplet transfer analysis in the first pattern indicates that the electromagnetic force significantly affects the droplet detachment mode. When the wire feed speed increases to 5.0 m min^{-1}, the curve that the wire feed rate equals the melting rate, shown as the red line in Fig. 8, moves to the right side, and thus the welding current increases and melts more wire mass to possibly resume to the original balance working point by the arc inherent self-regulation. However, the change of welding current does not stabilize the arc process but accelerates the climbing up of the arc attachment along the sidewalls, and finally, generates two arc conductive paths showed in Fig. 10. This arc shape pattern completely changes the distribution of the electromagnetic force on the droplet. When the arc burns between the wire tip and the bottom of the narrow gap, the root area of the arc is expanded, which can be observed in Fig. 10.

The electromagnetic force will accelerate the droplet detachment once the root area of the arc expands to the wire tip and wholly encompasses the droplet. The force F_e can be projected on

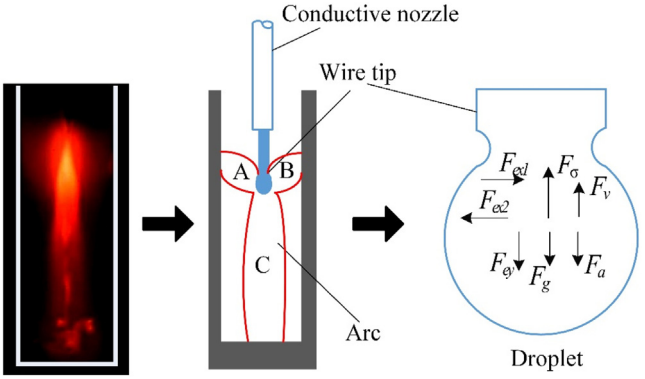

Fig. 11. Simplified arc shape and forces acted on the droplet in the third pattern.

the x and y axis. The vertical projection F_{ey} increases the acceleration force combined with the gravity and promotes the droplet detachment. The horizontal projection F_{ex} can accelerate the occurrence of the necking phenomenon, which further promotes the droplet detachment from the wire tip. Hence, in this arc shape pattern, the electromagnetic force is considered as an acceleration force for the droplet detachment such that the droplet size grows smaller. The variation of the droplet size is shown in Fig. 5.

3.4.3. Characteristics in the third pattern

As shown in Fig. 6, three arc conductive paths of the arc are generated between the wire tip and the bottom of the narrow gap as well as the right and left sidewalls. Thus, the distribution of the electromagnetic force acting on the droplet would be apparently changed. The schematic diagram is shown in Fig. 11.

The horizontal projections F_{ex1} (range A) and F_{ex2} (range B) of the electromagnetic force accelerate the occurrence of the necking process due to their inverse action. Two vertical projections F_{ey1} and F_{ey2} increase the combination of all electromagnetic forces in the axial direction and quicken the droplet detachment. These inferences can be explained and verified using Eq. (3) (detailed by Tipi et al. (2015)). Because the arc attachment points move to the range A and range B along the sidewalls, the root angle θ of the arc (shown in Fig. 9) is increased. Analysis of the right side of Eq. (3) indicates that the value of the electromagnetic force projected on the axial direction increases when the droplet diameter approximately keeps constant at a given time.

$$F_{em} = \frac{\mu_0 I^2}{4\pi}\left[\ln\frac{r_d \sin\theta}{r_w} - \frac{1}{1-\cos\theta} + \frac{2}{(1-\cos\theta)^2}\ln\frac{2}{1+\cos\theta}\right] \quad (3)$$

In Eq. (3), μ_0 is the vacuum magnetic conductivity. θ is the root angle of the arc. r_w is the wire radius. I is the welding current. r_d is the droplet radius.

In summary, another arc conductive path generated in the third arc shape pattern further increases the combination of all projections of the forces on axial direction such that both gravity and size of the droplet become smaller, which promotes the droplet detachment from the wire tip with a spray transfer mode.

3.5. Restricted arc modeling and simulation

The arc appearance in the narrow gap GMA welding process is classified and analyzed based on the change of the current path, and the corresponding metal transfer behaviors are studied based on the static force balance theory in pre-sections. To demonstrate the rationality and accuracy of the pre-assumption that using the current path distinguishes the arc appearance, a mathematical arc model in the narrow gap restricted condition was established, and its variation with the change of wire feed rate was simulated based on the MATLAB/Simulink platform. The arc conductive path was approximated to illustrate the modeling process simply, which was shown in Fig. 12.

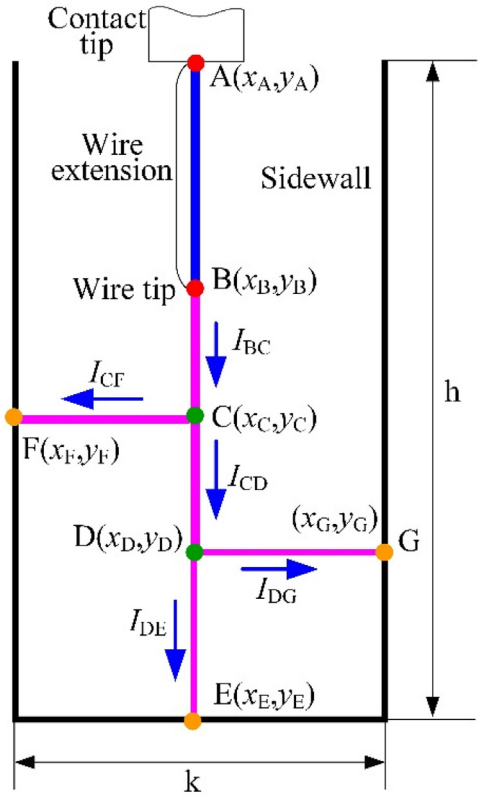

Fig. 12. Diagram of the approximated arc conductive path.

In order to simplify the mathematical arc model of the narrow gap GMAW, some assumptions have been made as follows:

(1) The total welding current originated from point B is divided into two paths at point C: one conducts to the sidewall remarked with CF line, and another conducts to point D denoted with CD line. The current flowing out from CD line is divided into two parts again: one path is DG line, and the other path is DE line. The correlation between the total current and the divided current satisfies the following equation.

$$I_{AB} = I_{BC} = I_{CF} + I_{DG} + I_{DE} \quad (4)$$

(2) The welding power source is an ideal constant-voltage power source (CVPS), and its energy consumption can be neglected.
(3) In the arc column field, the plasma conductive path is completely generated.
(4) The selection of the arc conductive path in the arc column field automatically follows the principle of minimum energy consumption. The arc conductive path is also simplified the linear path.
(5) The droplet size can be calculated using a spherical shape model.

The welding arc characteristics are described using Ayrton's equation (Choi et al., 2001).

$$U_a = k_1 + k_2 \cdot I + (k_3 + k_4 \cdot I) \cdot l_a \quad (5)$$

Where l_a denotes the arc length and the k denotes the constants depending on the welding wire and the shielding gas. The conventional wire equation has been used to describe the correlation

between the rate change of the wire extension, wire feed, and melting rate.

$$\frac{dL_e}{dt} = V_f - V_m and V_m = C_1 I + C_2 I^2 L_e \quad (6)$$

Where L_e represents the wire extension; V_f is the wire feed rate; V_m is the wire melting rate, and C_1 and C_2 represent the influence coefficient of arc length and joule heating, respectively.

The droplet size has an effect on the varying wire extension, which is considered for predicting the dynamic behavior of the NG-GMAW more precisely, hence, the Eq. (6) is modified to include the effect of a hanging droplet at the wire tip. The wire extension is described in this work as the sum of the solid extension length and molten droplet length hanging at the wire tip.

$$\frac{dL_{es}}{dt} = V_f - V_m \quad (7)$$

$$\frac{dV_d}{dt} = \left(\frac{\pi D_e^2}{4}\right) V_m \quad (8)$$

Where L_{es} represents the sum of the solid wire extension and the wire diameter; V_d is the attached droplet volume, and D_e is the wire diameter; the drop length can be calculated from the drop volume by the pre assumptions.

Consequently, each of the arc voltage supposed U_{BF}, U_{BG} and U_{BE} can be expressed using the Eq. (5).

$$U_{BF} = k_1 + k_2(I_{BC} + I_{CF}) + k_3(l_{BC} + l_{CF}) + k_4(I_{CF} l_{CF} + I_{BC} l_{BC}) \quad (9)$$

$$U_{BG} = k_1 + k_2(I_{BC} + I_{CD} + I_{DG}) + k_3(l_{BC} + l_{CD} + l_{DG}) + k_4(I_{CD} l_{CD} + I_{BC} l_{BC} + I_{DG} l_{DG}) \quad (10)$$

$$U_{BE} = k_1 + k_2(I_{BC} + I_{CD} + I_{DE}) + k_3(l_{BC} + l_{CD} + l_{DE}) + k_4(I_{CD} l_{CD} + I_{BC} l_{BC} + I_{DE} l_{DE}) \quad (11)$$

Where U_{BF} represents the arc voltage between the wire tip (point B) and the left attachment point F. U_{BG} is the arc voltage between the wire tip (point B) and the bottom of the narrow gap (point E). U_{BE} is the arc voltage between the wire tip (point B) and the right attachment point G. I_{BC} represents the current flowing from point B to C, and l_{BC} is the arc length of line BC. I_{CF} is the current flowing from point C to F, and l_{CF} is the arc length of point C to F. I_{CD} is the current flowing from point C to D, and l_{CD} is the arc length of point C to D. I_{DG} denotes the current flowing from point D to G, and l_{DG} is the arc length of point D to G. I_{DE} is the current flowing from point D to G. d_{DE} is the arc length of point D to E. k is the same value and unit in Eq. (5).

To this end, the arc model of the narrow gap GMAW is obtained and can be solved using the following constraint conditions as shown in Eq. (12).

$$\begin{cases} U_{BE} = U - U_{AB} \\ U = U_k + U_C + U_{AE} \\ U_{BF} = U_{BE} = U_{BG} \\ I_{BC} = I_{CF} + I_{CD} \\ I_{CD} = I_{DE} + I_{DG} \\ V_m = V_f \\ l_{CD} = \sqrt{(x_C - x_D)^2 + (y_C - y_D)^2} \\ l_{CF} = \min\left(x_{C,} k - x_C\right) \\ l_{DG} = \min\left(x_{D,} k - x_D\right) \\ d_{DE} = h - y_D \end{cases} \quad (12)$$

Before computing the arc conductive path distribution, the coordinates of points C and D are first initialized, respectively. The coordinates are updated by the boundary conditions. The results computed with Table 1 parameters are shown in Fig. 13.

Table 1
Corresponding parameters used in simulation.

Nomenclature	Value
Cathode fall voltage U_k (v)	8.7
Anode fall voltage U_c (v)	4.3
Density of solid phase ρ (kg m^{-3})	7800
Constant for arc heating C_1 mm/As	0.2940
Constant for joule heating C_2 A^{-2}s^{-1}	4.6081×10^{-5}
k_1 (V)	16.24
k_2 (Ω)	0.02376
k_3 (V/mm)	0.553
k_4 (V/Amm)	6.395×10^{-4}
Height of sidewall h (m)	0.04
Width of narrow gap k (m)	0.01
Welding current I_{bc} (A)	300
Wire feed rate V_f (m min^{-1})	4.3, 5.0, 6.0
Initialized wire extension L_e (m)	0.025

As shown in Fig. 13, the simulated results can match the experiments, and each of the arc conductive path varies with the change of wire extension. Fig. 13(a) corresponds to the first arc shape pattern showed in Fig. 4. It is apparently observed that most of the current (244A) originated from the wire tip (total 300A) flow to the sidewalls, and the reminder flow to the DE (14A) and DG (41A) paths. This current distribution easily forms the globular droplet transfer mode because of the large asymmetric electromagnetic force which linearly correlates to the value of the current. When the wire feed rate increases, the point dividing the arc conductive path is updated by the arc inherent self-regulation for satisfying the boundary conditions. Then, the result showed in Fig. 13(b) is obtained, which associates with the second arc shape pattern showed in Fig. 5. Fig. 13(b) indicates that the current flowing into the CF path decreases, instead of increasing the current of the DG path. When the third arc shape pattern showed in Fig. 13(c) and (d) is formed, the current flowing into the DG path further increases due to the action of the arc self-regulation, and thus the symmetrical arc shape is generated, which benefits to the droplet transfer and spray transfer mode production.

In summary, computation demonstrates that it is reasonable to elaborate the change of the arc shape in the narrow gap condition using the minimum arc voltage principle and arc inherent self-regulation, and the factors producing the different droplet transfer mode under different arc shape pattern mainly attribute to the change of the arc conductive path. The varying current path mainly changes the direction and dimension of the electromagnetic force acting on the droplet.

3.6. Analysis of the CCPS condition

It has been concluded, based on the analysis of the arc shape and metal transfer behavior in the CVPS applied-welding process, that the arc inherent self-regulation causes the climbing up phenomenon of the arc along the sidewalls, and produces various droplet transfer modes. The unstable metal transfer process leads to form the poor weld bead appearance. To reduce the effect of the arc inherent self-regulation on the arc stability, a welding system employed CCPS combining constant wire feed rate was developed, and several bead-on-plate experiments were conducted on the work-piece with the same dimension and structure showed in Fig. 1. Several typical images of the arc shape were shown in Fig. 14. During the welding process, the current was set 300A. ER50-6 wire with the diameter 1.2 mm was employed; wire feed rate was set 7.1 m min^{-1}, and the welding speed was set 0.325 m min^{-1}. Pure

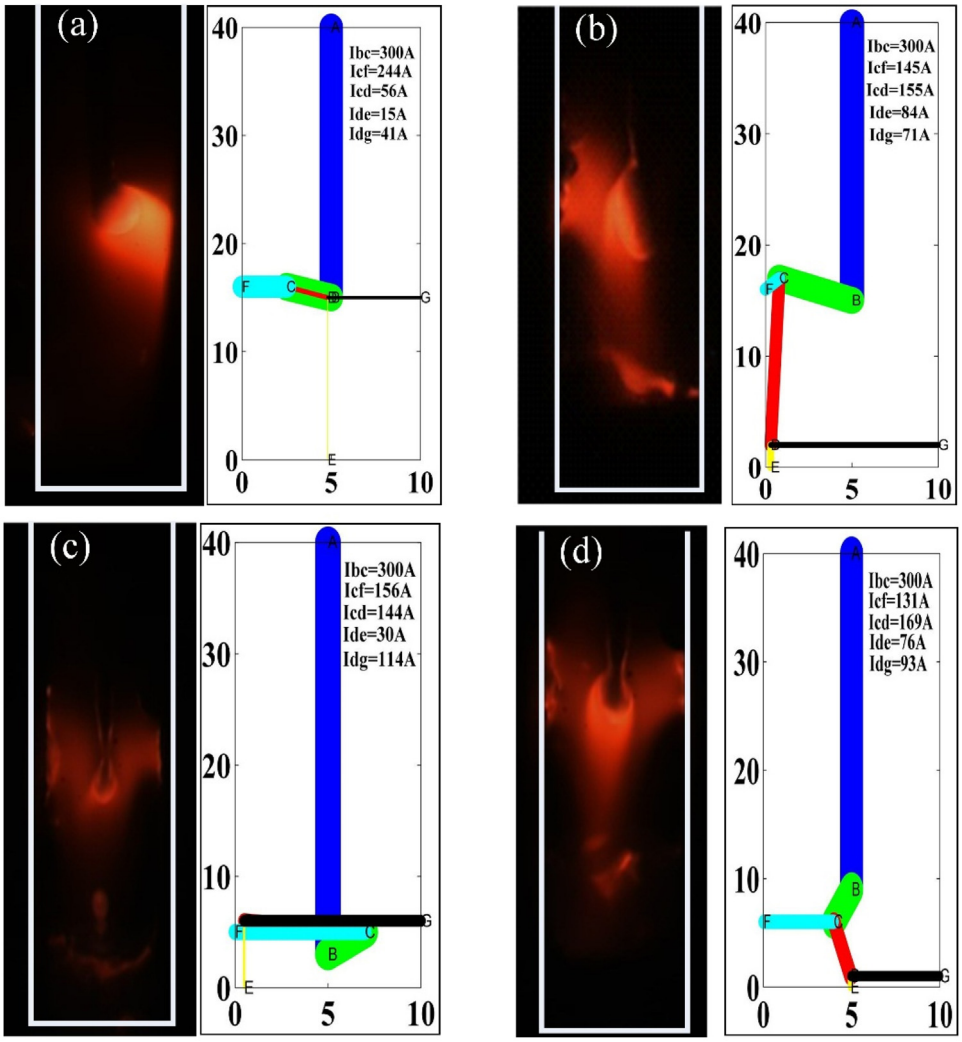

Fig. 13. Arc conductive path distribution (simulation and experiment).

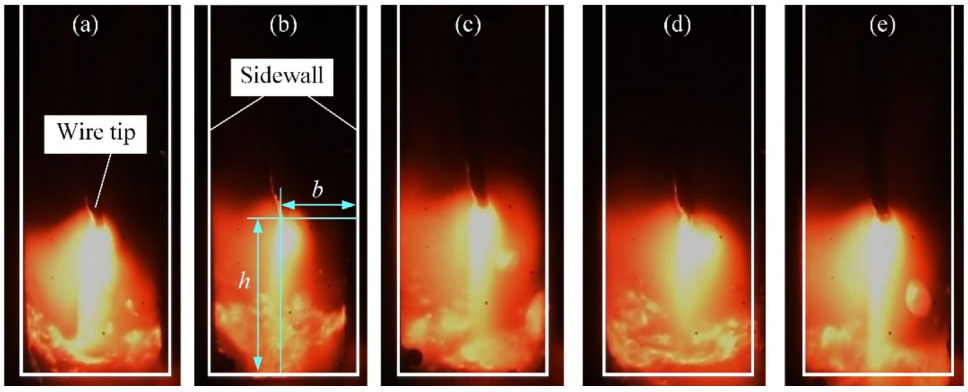

Fig. 14. Typical arc shape images captured in the CCPS condition (Selected at interval 0.5 s).

argon (99%) at a flow rate 10 L min^{-1} was also used as the shielding gas.

Fig. 14 depicts that the arc shape changes smaller than that showed in Figs. 4–6, and the wire extension is basically kept to the original length. The arc can steadily burn between the wire tip and the bottom of the narrow gap, and a stable welding process without the climbing up phenomenon of the arc is obtained. Interestingly, this result contradicts the CVPS case. The reasons can be derived from the analysis of the arc inherent self-regulation under the CCPS condition. The diagram of the arc inherent self-regulation is shown in Fig. 15.

Fig. 14 obviously shows that the vertical distance h of the wire tip to the bottom of the narrow gap is larger than the horizontal distance b of the wire tip to the right and left sidewalls. Based on the minimum arc voltage principle, the burning arc will choose the shortest conductive path to keep its minimum energy

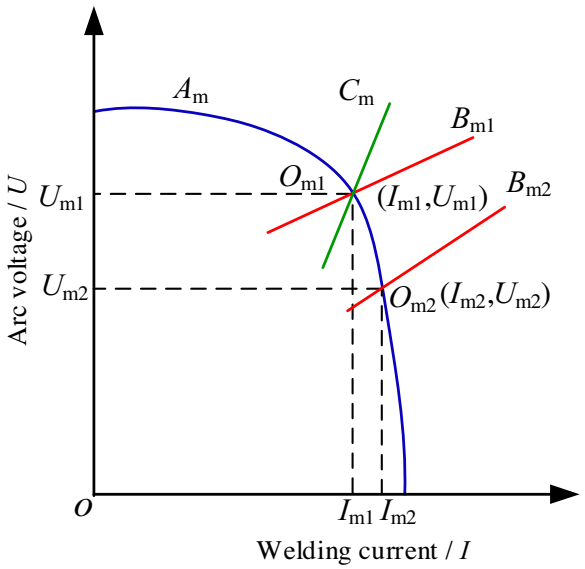

Fig. 15. Diagram of the arc inherent self-regulation under the CCPS condition.

consumption. Hence, the arc voltage linearly correlating to the arc length will be reduced, and the current will be increased when the arc attachment point moves from the bottom of the narrow gap to the sidewalls. These changes can be analyzed in Fig. 15. Such that, the balance working point of the burning arc will move from O_{m1} to O_{m2} for rebuilding another balance working point to stabilize the welding process. However, the small increase of welding current mainly depends on the outside-characteristic of the welding power source, and the arc voltage has a large decrease. The melting rate of the wire at the point O_{m2} increases. This conclusion can be verified by the Eq. (1). Finally, the burning arc shape resumes the original status, and the climbing up phenomenon of the arc is not generated. However, choosing an appropriate wire feed rate to match the given welding current is very difficult because the regulating range of the wire feed rate is very narrow. Hence, if the outside-characteristic of the welding power source cannot match the change in the wire feeding and melting rate very well, the short circuit or melting conductive nozzle phenomenon may occur. In addition, the dynamic response of the welding power source and the quality of the wire feed machine has a higher requirement for meeting this special condition. These requirements increase the cost of the welding production.

4. Conclusions

The arc characteristics and droplet transfer behavior of the narrow gap-restricted GMAW have been studied by experiments and simulation. The following conclusions can be drawn from this work.

(1) An improved rapid prototyping control system is employed to capture the arc dynamics and droplet transfer simultaneously.
(2) In a constant wire feed rate combined CVPS condition, the climbing up phenomenon of the arc along the sidewalls is observed, and three kinds of arc appearance are formed, producing globular transfer and spray transfer modes with the increase of wire feed rate.
(3) The minimum arc voltage principle combing with the arc inherent self-regulation results in the arc climbing up phenomenon.
(4) The varying arc shape directly changes the size and direction of the electromagnetic force acting on the droplet and significantly determines the droplet size and detachment. The electromagnetic force in the first arc shape pattern prevents the droplet transfer and produces a globular transfer mode. In the second arc shape pattern, the vertical projection of the electromagnetic force between the wire tip and the sidewall increases the combined force acting on the droplet and accelerates the occurrence of the necking process of the droplet detachment. A globular droplet transfer mode is obtained, and the droplet size becomes smaller. In the third arc shape pattern, three arc conductive paths between the wire tip to the sidewalls and the bottom of the narrow gap are formed, and the vertical projections of the electromagnetic force further increase such that the occurrence of the necking process of the droplet detachment becomes easier. A spray transfer mode is formed.
(5) The simulation results match the experiments and demonstrate that the mechanism proposed to elaborate the climbing up phenomenon of arc attachment is reasonable, and the change of the arc conductive path leads to the formation of the different metal transfer modes.
(6) In the CCPS case, the arc climbing up phenomenon hardly occurs due to the weak arc inherent self-regulation, and a stable welding process is finally obtained.

Acknowledgements

This work is funded by the National Natural Science Foundation of China [Grant Number 61365011, 2014]; Natural Science Foundation of Gansu Province of China [Grant Number 1508RJZA070, 2015]; Young Creative Talent Support Program of Long Yuan of China; State Key Laboratory of Advanced Processing and Recycling of Nonferrous Metals of China [Grant Number SKLAB02015008, 2015].

References

Amson, J.C., 1965. Lorentz force in the molten tip of an arc electrode. Br. J. Appl. Phys. 16, 1169–1179.
Cai, X.Y., Fan, C.L., Lin, S.B., Yang, C.L., Ji, X.R., Hu, L., 2016. Effects of shielding gas composition on arc characteristics and droplet transfer in tandem narrow gap GMA welding. Sci. Technol. Weld. Join. 92 (5), 1–8.
Cao, X., Wanjara, P., Huang, J., Munro, C., Nolting, A., 2011. Hybrid fiber laser–arc welding of thick section high strength low alloy steel. Mater. Des. 32 (6), 3399–3413.
Choi, J.H., Lee, J.U., Yoo, C.D., 2001. Simulation of dynamic behavior in a GMAW system. Weld. J. 90, 239s–245s.
Fan, H.G., Kovacevic, R., 2004. A unified model of transport phenomena in gas metal arc welding including electrode, arc plasma and molten pool. J. Phys. D: Appl. Phys. 37, 2531–2544.
Frank, V., Stefan, G., Michael, R., Andrey, G., Uwe, R.U., Simon, O., 2010. Welding thick steel plates with fibre lasers and GMAW. Weld. World 54 (3), 62–70.
Gan, W., Li, Z.T., Khurana, S., 2007. Tool materials selection for friction stir welding of L80 steel. Sci. Technol. Weld. Join. 12 (7), 610–613.
Guo, N., Han, Y.F., Jia, C.B., Du, Y.P., 2011. Effects of wire rotating frequency on metal transfer process in rotating arc narrow gap horizontal GMAW. Adv. Mater. Res. 189–193, 3395–3399.
Haidar, J., 1998. An analysis of the formation of metal droplets in arc welding. J. Phys. D: Appl. Phys. 31 (10), 1233–1244.
Kiran, D.V., Basu, B., De, A., 2012. Influence of process variables on weld bead quality in two wire tandem submerged arc welding of HSLA steel. J. Mater. Process. Technol. 212 (10), 2041–2050.
Lu, L.H., Fan, D., Huang, J.K., Shi, Y., 2012. Decoupling control scheme for pulsed GMAW process of aluminium. J. Mater. Process. Technol. 212, 801–807.
Tipi, A.R.D., Sani, S.K.H., Pariz, N., 2015. Frequency control of the drop detachment in the automatic GMAW process. J. Mater. Process. Technol. 216, 248–259.
Wang, J.Y., Zhu, J., Fu, P., Su, R.J., Han, W., Yang, F., 2012. A swing arc system for narrow gap GMA welding. ISIJ Int. 52 (1), 110–114.
Xu, W.H., Lin, S.B., Fan, C.L., Yang, C.L., 2014. Evaluation on microstructure and mechanical properties of high-strength low-alloy steel joints with oscillating arc narrow gap GMA welding. Int. J. Adv. Manuf. Technol. 75, 1439–1446.
Xu, W.H., Lin, S.B., Fan, C.L., Yang, C.L., 2015. Prediction and optimization of weld bead geometry in oscillating arc narrow gap all-position GMA welding. Int. J. Adv. Manuf. Technol. 79, 183–196.
Yang, C.L., Guo, N., Lin, S.B., Fan, C.L., Zhang, Y.Q., 2009. Application of rotating arc system to horizontal narrow gap welding. Sci. Technol. Weld. Join. 14 (2), 172–177.
Zhu, L., Zheng, S.X., Chen, J.H., 2006. Development of ultra-narrow gap welding with constrained arc by flux band. China Weld. 15 (2), 44–49.